Bioorganic & Medicinal Chemistry xxx (2018) xxx–xxx

Contents lists available at ScienceDirect

Bioorganic & Medicinal Chemistry

journal homepage: www.elsevier.com/locate/bmc

Design, synthesis, and biological evaluation of new B-Raf^{V600E} kinase inhibitors

Peng-Fei Wang [a], Yong-Jiao Zhang [a], Dong Wang [a,b], Hui-Min Hu [a], Zhong-Chang Wang [a], Chen Xu [a,*], Han-Yue Qiu [a,*], Hai-Liang Zhu [a,*]

[a] State Key Laboratory of Pharmaceutical Biotechnology, Nanjing University, Nanjing 210023, People's Republic of China
[b] State Key Laboratory of Natural Medicines, Key Laboratory of Drug Metabolism and Pharmacokinetics, China Pharmaceutical University, Nanjing 210009, People's Republic of China

ARTICLE INFO

Article history:
Received 13 December 2017
Revised 18 March 2018
Accepted 24 March 2018
Available online xxxx

Keywords:
B-Raf
Molecular dynamics
Docking
Kinase inhibitor
Drug design

ABSTRACT

The association of deregulated signal pathways with various diseases has long been a research hotspot. One of the most important signal pathways, the MAPK (mitogen-activated protein kinase) signal pathway, plays a vital role in transducing extracellular signals into vital intracellular mechanisms. While mutations on its key component Raf kinase lead to sever diseases, targeted inhibition has thereby become an attractive therapeutic strategy. Several drugs have been approved for the treatment of Raf relevant diseases, yet more candidates are ever needed as the known drugs have confronted resistance and side effects. In the present study, we primarily investigated the binding modes of type I/II and type II inhibitors with B-Raf kinase. Based on the current knowledge, these ligands were fragmented and recombined to provide new interesting insights. Afterwards, a series of derivatives has been synthesized after the validation of hit compound. In addition, *in vitro* assays were carried out to profile the pharmacological properties of all the entities. Of all the compounds, compound **5h** showed the best profile and may be used in the future study.

1. Introduction

The Raf kinase is a key ingredient in the ERK signaling branch of MAPK cascade and holds a central position in the signal transduction machinery.[1] Of its three family members, B-Raf kinase distributes more widely and functions more actively than the other two subtypes, i.e. A-Raf and c-Raf.[2] When pathological mutation occurs to the Raf kinase, it usually refers to the B-Raf subtype[3] Especially, when the VAL residue at site 600 mutated into an GLU residue, the kinase will mimic its activated state and persistently trigger downstream pathways.[4,5] Various malignant tumors are found to be related to mutated B-Raf kinase, for instance, most melanoma cases are caused by the B-Raf^{V600E} mutation.[6] Other somatic tumors, such as colorectal carcinoma and lung cancer, are also validated to be involved with the mutated B-Raf kinase.[7,8]

So far, great efforts have been dedicated to the development of potent B-Raf inhibitors, and several drugs have already been approved for the treatment of Raf-related diseases.[9] The most successful case is the gradual optimization for the final drug vemurafenib employing FBDD (Fragment-based Drug Design) strategy.[10] Compared with other known drugs (Fig. 1), such as dabrafenib and sorafenib, vemurafenib has a significant advantage in the Raf kinase selectivity.[11,12] It exhibits a much stronger inhibitory effect towards B-Raf kinase over the other two subtypes.[13] Hence, it's widely employed in the treatment of diseases caused by B-Raf^{V600E}. However, cases of relapse and resistance gradually increase with the use of vemurafenib.[14,15] The adverse effect caused by vemurafenib, on the other side, is also unneglectable.[16] As a classic type I/II kinase inhibitor, vemurafenib induces paradoxical effect in normal cells, i.e. enhancing the activity of wild type B-Raf kinase in low doses while suppressing it in high doses.[17] Hitherto, extensive studies have been carried out to reveal the underlying mechanism and to design new paradoxical breakers.[18,19]

It's of interest to note that among all the three types of inhibitors (targeting type I, type II and type I/II conformational kinases), the type II inhibitors have the minimal paradoxical inducing effects.[20] On this basis, modifying the other types of inhibitors into type II may yield optimized agents without paradoxical inducing effect. In this study, we primarily investigated the binding modes of type I/II and type II protein–ligand complexes. It has been noted that the major differences between them lie in the back pocket region, rather than in the front pocket region. Based on the analysis, the shared components for both two types' inhibitors in the

* Corresponding authors.
E-mail address: zhuhl@nju.edu.cn (H.-L. Zhu).

https://doi.org/10.1016/j.bmc.2018.03.038
0968-0896/

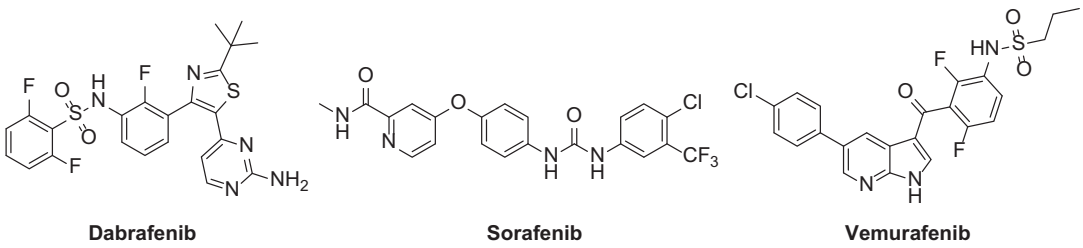

Fig. 1. Chemical structures of dabrafenib, sorafenib and vemurafenib.

front pocket region were validated. The recombination was then achieved to furnish several hybrids. Taking the binding score and synthesis accessibility into consideration, hit compound was selected and structurally modified. In addition, the validating molecular dynamics simulation helped to give further information. After chemical synthesis, 20 new entities were acquired and tested by *in vitro* assays. The results suggest some of the new compounds have good activity towards B-Raf^{V600E} kinase. Meanwhile, the same workflow may also be employed in other kinase inhibitor studies to avoid paradoxical effects with high efficiency.

2. Material and methods

2.1. Materials

All chemicals (reagent grade) used were purchased from Nanjing Chemical Reagent Co. Ltd. (Nanjing, China). Sorafenib was purchased from Sigma-Aldrich (St. Louis, MO). All the ^{1}H NMR spectra were recorded on a Bruker DPX 400 model spectrometer in DMSO d_6, and chemical shifts (d) are reported as parts per million (ppm). ESI-MS spectra were recorded by a Mariner System 5304 Mass spectrometer. Elemental analyses were performed on a CHN-O-Rapid instrument and were within 0.4% of the theoretical values. Melting points were determined on a XT4 MP apparatus (Taike Corp, Beijing, China). Thin layer chromatography (TLC) was performed on silica gel plates (Silica Gel 60 GF254) and visualized in UV light (254 nm and 365 nm). Column chromatography was performed using silica gel (200–300 mesh) and eluting with ethylacetate and petroleum ether (bp. 30–60 °C). A375 cells were kindly provided by Stem Cell Bank, Chinese Academy of Sciences. The other cell lines (WM266-4, WM1361, HT29 and HCT116) were preserved in the State Key Laboratory of Pharmaceutical Biotechnology of Nanjing University. The AnnexinV-FITC cell apoptosis assay kit was purchased from Vazyme Biotechco., Ltd (Nanjing, China). The Raf kinase was purchased from Invitrogen (US). All antibodies were obtained from WanleiBio (Shenyang, China).

2.2. Chemistry

2.2.1. Synthesis of ***2a-2b***

To a solution of **1a-1b** (4.5 mmol) in 4 mL ethanol was added 80% hydrazine hydrate (2 mL) and 10% palladium charcoal (0.08 g). The reaction was refluxed for 10 min and filtered by Celite. The filtrate was dried by sodium sulfate, and concentrated *in vacuo* to afford compounds **2a-2b**, which were used without further purification.

2.2.2. Synthesis of ***3a-3b***

Under stirring, 3-nitrobenzoic acid (2 mmol, 0.33 g), EDC (2 mmol, 0.38 g) and HOBT (2 mmol, 0.27 g) were added in 5 mL DMF. After reaction at rt for 30 min, the solution was added with DMAP (2 mmol, 0.24 g), **2a-2b** (2 mmol) and Et_3N (1 mL). The reaction mixture was stirred at rt for 18 h, before diluted with 20 mL of water and extracted with ethyl acetate. The organic layer was washed with aqueous saturated sodium bicarbonate, dried by sodium sulfate, filtered and concentrated *in vacuo*. Purification by flash chromatography gave the desired products **3a-3b**.

2.2.3. Synthesis of ***4a-4b***

To a solution of **3a-3b** (1.8 mmol) in 2 mL ethanol was added 80% hydrazine hydrate (1 mL) and 10% palladium charcoal (0.03 g). The reaction was refluxed for 10 min and filtered by Celite. The filtrate was dried by sodium sulfate, and concentrated *in vacuo* to afford compounds **4a-4b**, which were used without further purification.

2.2.4. Synthesis of ***5a-5t***

Under stirring, substituted nitrobenzoic acids (1.5 mmol), EDC (1.5 mmol, 0.38 g) and HOBT (1.5 mmol, 0.2 g) were added in 4 mL DMF. After reaction at rt for 30 min, the solution was added with DMAP (1.5 mmol, 0.18 g), **4a-4b** (1.5 mmol) and Et_3N (0.8 mL). The reaction mixture was stirred at rt for 18 h, before diluted with 20 mL of water and extracted with ethyl acetate. The organic layer was washed with aqueous saturated sodium bicarbonate, dried by sodium sulfate, filtered and concentrated *in vacuo*. Purification by flash chromatography gave the desired products **5a-5t**.

*2.2.4.1. 3-Benzamido-N-(1H-indazol-5-yl)benzamide (**5a**).* White solid, yield 88.1%, m.p. 285.2–286.9 °C. ^{1}H NMR (400 MHz, DMSO d_6) δ 13.03 (s, 1H, NH), 10.48 (s, 1H, NH), 10.32 (s, 1H, NH), 8.35 (s, 1H, ArH), 8.27 (s, 1H, CH), 8.04 (dd, J = 20.2, 9.5 Hz, 4H, ArH), 7.73 (d, J = 7.7 Hz, 1H, ArH), 7.64 (dd, J = 19.6, 8.1 Hz, 2H, ArH), 7.59–7.51 (m, 4H, ArH). MS EI$^+$: 356.39 ($C_{21}H_{16}N_4O_2$, [M]$^+$). Anal. Calcd: C, 70.77; H, 4.53; N, 15.72; Found: C, 70.57; H, 4.68; N, 15.83.

*2.2.4.2. N-(3-((1H-Indazol-5-yl)carbamoyl)phenyl)-3-fluorobenzamide (**5b**).* White solid, yield 73.5%, m.p. 293.6–295.2 °C. ^{1}H NMR (600 MHz, DMSO d_6) δ 13.03 (s, 1H, NH), 10.54 (s, 1H, NH), 10.32 (s, 1H, NH), 8.30 (d, J = 42.5 Hz, 2H, ArH), 8.08 (s, 1H, CH), 8.04 (d, J = 8.0 Hz, 1H, ArH), 7.87 (d, J = 7.8 Hz, 1H, ArH), 7.83 (d, J = 9.7 Hz, 1H, ArH), 7.75 (d, J = 7.7 Hz, 1H, ArH), 7.67–7.60 (m, 2H, ArH), 7.57–7.51 (m, 2H, ArH), 7.48 (td, J = 8.5, 2.2 Hz, 1H, ArH). MS EI$^+$: 374.38 ($C_{21}H_{15}FN_4O_2$, [M]$^+$). Anal. Calcd: C, 67.37; H, 4.04; N, 14.97; Found: C, 67.53; H, 4.13; N, 15.21.

*2.2.4.3. N-(3-((1H-Indazol-5-yl)carbamoyl)phenyl)-3-chlorobenzamide (**5c**).* Grey solid, yield 80.8%, m.p. 282.3–284.1 °C. ^{1}H NMR (600 MHz, DMSO d_6) δ 13.03 (s, 1H, NH), 10.71 (s, 1H, NH), 10.33 (s, 1H, NH), 8.97 (s, 1H, ArH), 8.32–8.25 (m, 3H, ArH and CH), 8.08 (s, 1H, ArH), 8.03 (d, J = 8.0 Hz, 1H, ArH), 7.88 (d, J = 8.3 Hz, 1H, ArH), 7.77 (d, J = 7.7 Hz, 1H, ArH), 7.65 (d, J = 10.3 Hz, 1H, ArH), 7.57–7.52 (m, 2H, ArH). MS EI$^+$: 390.83 ($C_{21}H_{15}ClN_4O_2$, [M]$^+$). Anal. Calcd: C, 64.54; H, 3.87; N, 14.34; Found: C, 64.32; H, 3.83; N, 14.42.

*2.2.4.4. 3-(4-Fluorobenzamido)-N-(1H-indazol-5-yl)benzamide (**5d**).* White solid, yield 71.8%, m.p. 294.7–296.5 °C. ^{1}H NMR (600 MHz, DMSO d_6) δ 13.04 (s, 1H, NH), 10.41 (d, J = 105.6 Hz, 2H, NH), 8.34 (s, 1H, ArH), 8.27 (s, 1H, CH), 8.18–7.97 (m, 4H, ArH), 7.74 (d, J = 7.4 Hz, 1H, ArH), 7.66 (d, J = 8.7 Hz, 1H, ArH), 7.53 (t, J = 8.0 Hz, 2H, ArH), 7.40 (t, J = 8.8 Hz, 2H, ArH). MS EI$^+$: 374.38 ($C_{21}H_{15}FN_4O_2$, $[M]^+$). Anal. Calcd: C, 66.37; H, 4.04; N, 14.97; Found: C, 66.06; H, 4.12; N, 14.96.

*2.2.4.5. 3-(4-Chlorobenzamido)-N-(1H-indazol-5-yl)benzamide (**5e**).* White solid, yield 76.1%, m.p. 296.5–298.6 °C. ^{1}H NMR (600 MHz, DMSO d_6) δ :13.03 (s, 1H, NH), 10.54 (s, 1H, NH), 10.32 (s, 1H, NH), 8.33 (s, 1H, ArH), 8.26 (s, 1H, CH), 8.08 (s, 1H, ArH), 8.04 (t, J = 7.4 Hz, 3H, ArH), 7.74 (d, J = 7.8 Hz, 1H, ArH), 7.65 (t, J = 8.7 Hz, 3H, ArH), 7.53 (t, J = 7.9 Hz, 2H, ArH). MS EI$^+$: 406.83($C_{21}H_{15}ClN_4O_3$, $[M]^+$). Anal. Calcd: C, 64.54; H, 3.87; N, 14.34; Found: C, 64.81; H, 3.83; N, 13.91.

*2.2.4.6. 3-(4-Bromobenzamido)-N-(1H-indazol-5-yl)benzamide (**5f**).* Grey solid, yield 82.3%, m.p. 286.7–287.9 °C. ^{1}H NMR (600 MHz, DMSO d_6) δ 13.03 (s, 1H, NH), 10.54 (s, 1H, NH), 10.31 (s, 1H, NH), 8.32 (s, 1H, ArH), 8.26 (s, 1H, CH), 8.08 (s, 1H, ArH), 8.03 (d, J = 8.0 Hz, 1H, ArH), 7.97 (d, J = 8.4 Hz, 2H, ArH), 7.78 (d, J = 8.4 Hz, 2H, ArH), 7.76–7.73 (m, 1H, ArH), 7.65 (d, J = 8.8 Hz, 1H, ArH), 7.56–7.51 (m, 2H, ArH). MS EI$^+$: 435.28 ($C_{21}H_{15}BrN_4O_2$, $[M]^+$). Anal. Calcd: C, 57.95; H, 3.47; N, 12.87; Found: C, 57.91; H, 3.53; N, 12.75.

*2.2.4.7. 3-(4-(Tert-butyl)benzamido)-N-(1H-indazol-5-yl)benzamide (**5g**).* White solid, yield 73.3%, m.p. 253.1–255.0 °C. ^{1}H NMR (600 MHz, DMSO d_6) δ 13.03 (s, 1H, NH), 10.39 (s, 1H, NH), 10.31 (s, 1H, NH), 8.34 (s, 1H, ArH), 8.27 (s, 1H, CH), 8.08 (s, 1H, ArH), 8.04 (d, J = 7.7 Hz, 1H, ArH), 7.95 (d, J = 8.4 Hz, 2H, ArH), 7.72 (d, J = 7.7 Hz, 1H, ArH), 7.66 (d, J = 8.8 Hz, 1H, ArH), 7.57 (d, J = 8.4 Hz, 2H, ArH), 7.55–7.51 (m, 2H, ArH), 1.34 (s, 9H, CH). MS EI$^+$: 356.39 ($C_{25}H_{24}N_4O_2$, $[M]^+$). Anal. Calcd: C, 72.80; H, 5.86; N, 13.58; Found: C, 72.68; H, 5.89; N, 13.62.

*2.2.4.8. N-(1H-Indazol-5-yl)-3-(4-(trifluoromethyl)benzamido)benzamide (**5h**).* Yellow solid, yield 52.9%, m.p. 285.2–287.1 °C. ^{1}H NMR (600 MHz, DMSO d_6) δ 13.06 (s, 1H, NH), 10.74 (s, 1H, NH), 10.35 (s, 1H, NH), 8.36 (s, 1H, ArH), 8.27 (s, 1H, CH), 8.22 (d, J = 8.1 Hz, 2H, ArH), 8.08–8.04 (m, 2H, ArH), 7.94 (d, J = 8.4 Hz, 2H, ArH), 7.77 (d, J = 7.8 Hz, 1H, ArH), 7.66 (d, J = 8.6 Hz, 1H, ArH), 7.55 (t, J = 8.0 Hz, 2H, ArH). MS EI$^+$: 424.38 ($C_{22}H_{15}F_3N_4O_2$, $[M]^+$). Anal. Calcd: C, 62.26; H, 3.56; N, 13.20; Found: C, 62.32; H, 3.48; N, 13.21.

*2.2.4.9. N-(1H-Indazol-5-yl)-3-(4-phenoxybenzamido)benzamide (**5i**).* White solid, yield 85.1%, m.p. 298.2–299.3 °C. ^{1}H NMR (600 MHz, DMSO d_6) δ 13.04 (s, 1H, NH), 10.48 (s, 1H, NH), 10.25 (s, 1H, NH), 8.16 (d, J = 1.4 Hz, 1H, CH), 8.07 (d, J = 7.7 Hz, 2H, ArH), 7.96–7.89 (m, 2H, ArH), 7.86 (dd, J = 7.5, 1.6 Hz, 1H, ArH), 7.76–7.64 (m, 3H, ArH), 7.45 (t, J = 7.5 Hz, 1H, ArH), 7.39 (t, J = 7.5 Hz, 2H, ArH), 7.23–7.18 (m, 2H, ArH), 7.14 (tt, J = 7.3, 2.0 Hz, 1H, ArH), 7.05 (dd, J = 7.6, 2.0 Hz, 2H, ArH). MS EI$^+$: 448.48 ($C_{27}H_{20}N_4O_3$, $[M]^+$). Anal. Calcd: C, 72.31; H, 4.50; N, 12.49; Found: C,71.31; H, 4.63; N, 12.57.

*2.2.4.10. N-(3-((1H-Indazol-5-yl)carbamoyl)phenyl)picolinamide (**5j**).* White solid, yield 67.3%, m.p. 294.8–296.1 °C. ^{1}H NMR (600 MHz, DMSO d_6) δ 13.06 (s, 1H, NH), 10.71 (s, 1H, NH), 10.34 (s, 1H, NH), 9.17 (d, J = 1.8 Hz, 1H, ArH), 8.79 (dd, J = 4.8, 1.5 Hz, 1H, ArH), 8.38–8.34 (m, 2H, ArH), 8.27 (s, 1H, CH), 8.08–8.03 (m, 2H, ArH), 7.77 (d, J = 7.7 Hz, 1H, ArH), 7.66 (d, J = 7.7 Hz, 1H, ArH), 7.60 (dd, J = 7.8, 4.8 Hz, 1H, ArH), 7.55 (t, J = 7.7 Hz, 2H, ArH). MS EI$^+$: 357.37 ($C_{20}H_{15}N_5O_2$, $[M]^+$). Anal. Calcd: C, 67.22; H, 4.23; N, 19.60; Found: C, 67.27; H, 4.29; N, 19.53.

*2.2.4.11. N-(3-((1H-Indazol-5-yl)carbamoyl)phenyl)-6-methylpicolinamide (**5k**).* Yellow solid, yield 77.4%, m.p. 291.5–292.7 °C. ^{1}H NMR (600 MHz, DMSO d_6) δ 13.06 (s, 1H, NH), 10.61 (s, 1H, NH), 10.34 (s, 1H, NH), 9.06 (s, 1H, ArH), 8.34 (s, 1H, ArH), 8.29–8.25 (m, 2H, ArH and CH), 8.07 (s, 1H, ArH), 8.05–8.02 (m, 1H, ArH), 7.76 (d, J = 7.7 Hz, 1H, ArH), 7.66 (d, J = 10.0 Hz, 1H, ArH), 7.56–7.51 (m, 2H, ArH), 7.44 (d, J = 8.1 Hz, 1H, ArH), 2.57 (s, 3H, CH). MS EI$^+$: 371.40 ($C_{21}H_{17}N_5O_2$, $[M]^+$). Anal. Calcd: C, 67.91; H, 4.61; N, 18.86; Found: C, 67.88; H, 4.63; N, 18.82.

*2.2.4.12. N-(3-((1H-Indazol-5-yl)carbamoyl)phenyl)-6-chloropicolinamide (**5l**).* Yellow solid, yield 59.8%, m.p. 290.5–292.6 °C. ^{1}H NMR (600 MHz, DMSO d_6) δ 13.05 (s, 1H, NH), 10.75 (s, 1H, NH), 10.34 (s, 1H, NH), 9.01 (d, J = 2.4 Hz, 1H, ArH), 8.42 (dd, J = 8.3, 2.5 Hz, 1H, ArH), 8.32 (s, 1H, ArH), 8.26 (s, 1H, CH), 8.08 (s, 1H, ArH), 8.03 (d, J = 9.3 Hz, 1H, ArH), 7.78 (d, J = 7.7 Hz, 1H, ArH), 7.74 (d, J = 8.3 Hz, 1H, ArH), 7.65 (d, J = 8.9 Hz, 1H, ArH), 7.57–7.53 (m, 2H, ArH). MS EI$^+$: 391.08 ($C_{20}H_{14}ClN_5O_2$, $[M]^+$). Anal. Calcd: C, 61.31; H, 3.60; N, 17.87; Found: C, 61.36; H, 3.54; N, 17.79.

*2.2.4.13. N-(3-((1H-Indazol-5-yl)carbamoyl)phenyl)-5-bromopicolinamide (**5m**).* Grey solid, yield 56.8%, m.p.297.8–299.6 °C. ^{1}H NMR (600 MHz, DMSO d_6) δ 13.03 (s, 1H, NH), 10.72 (s, 1H, NH), 10.33 (s, 1H, NH), 9.12 (s, 1H), 8.94 (s, 1H, ArH), 8.61 (s, 1H, ArH), 8.31 (s, 1H, ArH), 8.26 (s, 1H, CH), 8.08 (s, 1H, ArH), 8.04 (d, J = 7.9 Hz, 1H, ArH), 7.78 (d, J = 7.7 Hz, 1H, ArH), 7.66 (d, J = 8.8 Hz, 1H, ArH), 7.58–7.53 (m, 2H, ArH). MS EI$^+$: 436.27 ($C_{20}H_{14}BrN_5O_2$, $[M]^+$). Anal. Calcd: C, 55.06; H, 3.23; N, 16.05; Found: C, 54.97; H, 3.41; N, 15.89.

*2.2.4.14 N-(3-((1H-Indazol-5-yl)carbamoyl)phenyl)-4-chloropicolinamide (**5n**).* White solid, yield 74.5%, m.p. 296.4–298.2 °C. ^{1}H NMR (600 MHz, DMSO d_6) δ 13.05 (s, 1H, NH), 10.56 (s, 1H, NH), 10.33 (s, 1H, NH), 8.33 (s, 1H, ArH), 8.26 (s, 1H, CH), 8.05 (q, J = 9.2 Hz, 4H, ArH), 7.64 (d, J = 8.6 Hz, 3H, ArH), 7.53 (t, J = 8.0 Hz, 2H, ArH). MS EI+: 391.08 ($C_{20}H_{14}ClN_5O_2$, $[M]^+$). Anal. Calcd: C, 61.31; H, 3.60; N, 17.87; Found: C, 61.36; H, 3.58; N, 17.84.

*2.2.4.15. 3-(((3-Chlorobenzoyl)oxy)amino)-N-(1H-indazol-5-yl)benzamide (**5o**).* White solid, yield 72.2%, m.p. 294.8–296.3 °C. ^{1}H NMR (600 MHz, DMSO d_6) δ 13.04 (s, 1H, NH), 10.55 (s, 1H, NH), 10.33 (s, 1H, NH), 8.29 (t, J = 2.0 Hz, 1H, ArH), 8.24 (d, J = 1.5 Hz, 1H, CH), 8.11–8.04 (m, 2H, ArH), 7.99 (dt, J = 7.5, 2.1 Hz, 1H, ArH), 7.72–7.61 (m, 3H, ArH), 7.29–7.20 (m, 4H, ArH). MS EI$^+$: 406.83 ($C_{21}H_{15}ClN_4O_3$, $[M]^+$). Anal. Calcd: C, 62.00; H, 3.72; N, 13.77; Found: C, 62.48; H, 3.57; N, 13.71.

*2.2.4.16. 3-Benzamido-N-(1H-indol-5-yl)benzamide (**5p**).* White solid, yield 57.9%, m.p. 175.5–177.3 °C. ^{1}H NMR (600 MHz, DMSO d_6) δ 11.05 (s, 1H, NH), 10.46 (s, 1H, NH), 10.13 (s, 1H, NH), 8.33 (s, 1H, ArH), 8.07–7.97 (m, 4H, ArH), 7.73 (d, J = 7.7 Hz, 1H, ArH), 7.62 (t, J = 7.3 Hz, 1H, ArH), 7.56 (t, J = 7.5 Hz, 2H, ArH), 7.52 (t, J = 7.9 Hz, 1H, ArH), 7.41 (dd, J = 8.7, 1.7 Hz, 1H, ArH), 7.37 (d, J = 8.6 Hz, 1H, ArH), 7.34 (t, J = 2.7 Hz, 1H, CH), 6.43 (s, 1H, CH). MS EI$^+$: 357.41 ($C_{22}H_{19}N_3O_2$, $[M]^+$). Anal. Calcd: C, 73.93; H, 5.36; N, 11.76; Found: C, 73.81; H, 4.98; N, 11.51.

*2.2.4.17. 3-(4-Chlorobenzamido)-N-(1H-indol-5-yl)benzamide (**5q**).* White solid, yield 65.5%, m.p. 214.1–216.3 °C. ^{1}H NMR (600 MHz, DMSO d_6) δ 11.05 (s, 1H, NH), 10.52 (s, 1H, NH), 10.12 (s, 1H, NH), 8.31 (s, 1H), 8.07–7.99 (m, 4H, ArH), 7.74 (d, J = 7.6 Hz, 1H, ArH), 7.64 (d, J = 8.5 Hz, 2H, ArH), 7.52 (t, J = 7.9 Hz, 1H, ArH), 7.41 (d, J = 8.7 Hz, 1H, ArH), 7.37 (d, J = 8.6 Hz, 1H, ArH), 7.34 (t, J

= 2.6 Hz, 1H, CH), 6.43 (s, 1H, CH). MS EI$^+$: 374.38 ($C_{22}H_{16}ClN_3O_2$, $[M]^+$). Anal. Calcd: C, 67.78; H, 4.14; N, 10.78; Found: C, 67.49; H, 4.23; N, 10.51.

*2.2.4.18. N-(1H-Indol-5-yl)-3-(4-phenoxybenzamido)benzamide (**5r**).* White solid, yield 54.9%, m.p. 148.8–150.6 °C. ^{1}H NMR (600 MHz, DMSO d_6) δ 11.05 (s, 1H, NH), 10.40 (s, 1H, NH), 10.12 (s, 1H, NH), 8.31 (s, 1H, ArH), 8.06 (d, J = 8.8 Hz, 2H, ArH), 8.04–7.99 (m, 2H, ArH), 7.72 (d, J = 7.7 Hz, 1H, ArH), 7.49 (dt, J = 21.9, 8.2 Hz, 3H, ArH), 7.41 (dd, J = 8.7, 1.7 Hz, 1H, ArH), 7.37 (d, J = 8.7 Hz, 1H, ArH), 7.34 (t, J = 2.7 Hz, 1H, ArH), 7.24 (t, J = 7.4 Hz, 1H, ArH), 7.13 (t, J = 8.7 Hz, 4H, CH), 6.43 (s, 1H, CH). MS EI$^+$: 449.51 ($C_{28}H_{23}N_3O_3$, $[M]^+$). Anal. Calcd: C, 74.82; H, 5.16; N, 9.35; Found: C, 74.66; H, 5.03; N, 9.28.

*2.2.4.19. N-(3-((1H-Indol-5-yl)carbamoyl)phenyl)picolinamide (**5s**).* White solid, yield 88.6%, m.p. 204.5–206.4 °C. ^{1}H NMR (600 MHz, DMSO d_6) δ 11.05 (s, 1H, NH), 10.65 (s, 1H, NH), 10.14 (s, 1H, NH), 9.16 (d, J = 1.7 Hz, 1H, ArH), 8.79 (dd, J = 4.8, 1.6 Hz, 1H, ArH), 8.35 (dt, J = 7.9, 1.9 Hz, 1H, ArH), 8.32 (s, 1H, ArH), 8.09–7.95 (m, 2H, ArH), 7.75 (d, J = 7.8 Hz, 1H, ArH), 7.60 (dd, J = 7.9, 4.8 Hz, 1H, ArH), 7.53 (t, J = 7.9 Hz, 1H, ArH), 7.41 (dd, J = 8.7, 1.8 Hz, 1H, ArH), 7.37 (d, J = 8.6 Hz, 1H, ArH), 7.34 (t, J = 2.7 Hz, 1H, CH), 6.43 (s, 1H, CH). MS EI$^+$: 356.39 ($C_{21}H_{16}N_4O_2$, $[M]^+$). Anal. Calcd: C, 70.38; H, 5.06; N, 15.63; Found: C, 70.33; H, 4.97; N, 15.52.

*2.2.4.20. N-(3-((1H-Indol-5-yl)carbamoyl)phenyl)-6-chloropicolinamide (**5t**).* White solid, yield 55.8%, m.p. 169.1–171.3 °C. ^{1}H NMR (600 MHz, DMSO d_6) δ 11.06 (s, 1H, NH), 10.70 (s, 1H, NH), 10.15 (s, 1H, NH), 9.01 (s, 1H, ArH), 8.41 (dd, J = 8.3, 2.5 Hz, 1H, ArH), 8.30 (s, 1H, ArH), 8.01 (q, J = 8.4, 7.3 Hz, 2H, ArH), 7.76 (dd, J = 18.6, 8.1 Hz, 2H, ArH), 7.54 (t, J = 7.9 Hz, 1H, ArH), 7.41 (d, J = 8.8 Hz, 1H, ArH), 7.37 (d, J = 8.6 Hz, 1H, ArH), 7.35–7.33 (m, 1H, CH), 6.44–6.42 (m, 1H, CH). MS EI$^+$: 390.83 ($C_{21}H_{15}ClN_4O_2$, $[M]^+$). Anal. Calcd: C, 64.54; H, 3.87; N, 14.34; Found: C, 65.51; H, 3.85; N, 14.39.

2.3. Virtual simulation

The docking simulation was achieved by Accelrys Discovery Studio version 3.5 and complemented by Maestro 10.1. All the new compounds were docked into B-Raf (PDB code: 3IDP and 3C4C) binding site by CDOCKER. The binding results were further checked by SP, XP Glide and Flexible Dock according to the protocols. To verify whether the binding models were reliable, MD simulations were carried out using the GROMACS package (version 5.1.2) with GPU-accelerating support. The parameter setting and operating procedure can be seen in previous reports.[21,22]

2.4. Biological assays

2.4.1. Kinase activity inhibition

The V600E mutant B-Raf kinase assay was performed in triplicate for each tested compound in this study. Briefly, 7.5 ng Mouse Full-Length GST-tagged B-Raf V600E was pre-incubated at room temperature for 1 h with 1 μL drug and 4 μL assay dilution buffer. The kinase assay was initiated when 5 μL of a solution containing 200 ng recombinant human full length, *N*-terminal His-tagged MEK1, 200 μM ATP, and 30 mM $MgCl_2$ in assay dilution buffer was added. The kinase reaction was allowed to continue at room temperature for 25 min and was then quenched with 5 μL 5 × protein denaturing buffer (LDS) solution. Protein was further denatured by heating for 5 min at 70 °C. 10 μL of each reaction was loaded into a 15-well, 4–12% precast NuPage gel and run at 200 V, and upon completion, the front, which contained excess hot ATP, was cut from the gel and discarded. The gel was then dried and developed onto a phosphor screen. A reaction that contained no active enzyme was used as a negative control, and a reaction without inhibitor was used as the positive control.

2.4.2. Cell culture

Four cancer cell lines were used in this work: human melanoma cells A375 (B-Raf^{V600E} mutated), WM266-4 (B-Raf^{V600E} mutated) and WM1361 (B-Raf^{WT}), human colon cancer cells HT29 (B-Raf^{V600E} mutated) and HCT116 (B-Raf^{WT}). All cell lines were grown in Dulbecco's modified Eagle's medium (DMEM Hyclone), except for A375, which was maintained in DMEM 12,430 (Invitrogen) with Sodium Pyruvate (Invitrogen, 11360–070) added. All media were supplemented with 10% foetal bovine serum (FBS, BI), 2 mmol/L of l-glutamine, 100 units/mL of penicillin–streptomycin (Sigma-Aldrich), 100 mg/mL streptomycin (Hyclone) and incubated at 37 °C in a humidified atmosphere containing 5% CO_2.

2.4.3. Anti-proliferation assay

The anti-proliferative activities of the prepared compounds against the A375, WM266-4, WM1361, HT-29 and HCT116 were evaluated using a standard (MTT)-based colorimetric assay with some modification. Cell lines were grown to log phase in DMEM supplemented with 10% foetal bovine serum. Cell suspensions were prepared and 100 μL/well dispensed into 96-well plates to give 10^4 cells/well. After incubation for 24 h, cells were treated with the target compounds at 0.01, 0.1, 1, 10 and 100 μM in the presence of 10% FBS for 48 h. Afterwards, cell viability was assessed by the conventional 3-(4, 5-dimethylthiazol-2-yl)-2, 5-diphenyltetrazolium bromide (MTT) reduction assay carried out strictly according to the manufacturer's instructions (Sigma). The absorbance (OD_{570}) was read on an ELISA reader (Tecan, Austria). In all experiments, three replicate wells were used for each drug concentration. Each assay was performed at least three times.

2.4.4. Cell apoptosis

Approximately 10^5 cells/well were seeded in a 24-well plate and allowed to adhere. Subsequently, the medium was replaced with fresh culture medium containing the target compound at final concentrations of 0, 1, 2 and 4 μM. Non-treated wells received an equivalent volume of ethanol (<0.1%). After 24 h, the cells were trypsinized, washed twice with PBS and centrifuged at 2000 rpm for 5 min. The pellet was resuspended in 500 μL staining solution (containing 5 μL AnnexinV-FITC and 5 μL PI in Binding Buffer), mixed gently and incubated for 15 min at room temperature in dark. The cells were then analysed by a FACSCalibur flow cytometer (Becton Dickinson, San Jose, CA, USA).

2.4.5. Western blot analysis

Cells on 6-well plates were rinsed twice with cold PBS and lysed in RIPA lysis buffer containing a protease inhibitor (PMSF) mixture at 1:100 dilution on ice for 30 min. The insoluble components of cell lysates were removed by centrifugation (4 °C, 12,000×*g*, 10 min), and protein concentrations were measured using a Pierce BCA protein assay kit. Proteins were separated by sodium dodecyl sulfate–polyacrylamide gel electrophoresis (SDS-PAGE) and transferred onto polyvinylidene difluoride (PVDF) membranes. Membranes were blocked with 5% skim milk in 1×TBST buffer for 1 h at room temperature, and then incubated with corresponding primary antibodies diluted in 5% milk-TBST solution (1:500–1:1000 dilution) at 4 °C with gentle shaking overnight. After washing five times (5 min each) with 1×TBST, corresponding HRP-conjugated secondary antibodies (1:5000–1:10000 dilution) were incubated for 1 h at room temperature. Immunoreactive bands were visualized using an ECL detection kit (Invitrogen, USA) following the manufacturer's instruction.

3. Results and discussion

3.1. Data retrieval and analysis

As a typical kinase, B-Raf protein generally takes on three different conformations, which are type I, type II and type I/II states. While the front pocket (FP) region basically maintains the same when the kinase transforms from a conformation into another, the back pocket (BP) region is rather changeable in volume, shape and number of sub-pockets.[23] Accordingly, known inhibitors targeting B-Raf can be classified as three types depending on the protein conformations.[24] Based on this theory of knowledge, we gathered and grouped all the known co-crystals of B-Raf protein with ligand. Afterwards, all the complexes were superimposed by a same template protein which has the finest resolution (PDB code: 3IDP). It's not surprising that many inhibitors of the same type share similar structural features and interaction mode (Fig. 2). Notably, for the type I/II inhibitors, many bear a substituted sulfonamide group in the BP region interacting with residues LEU505, LEU 514, ASP594 and PHE595; while for the type II inhibitors, the mainstream chemical group in the BP region is a phenylurea or a benzamide group interacting with residues GLU501, VAL504, ILE572, HIS 574 and ASP594. Besides, these two types of ligands possess an overlapping phenyl group in space. Through this phenyl group, these ligands could be hybridized to provide new compounds. In this study, we intended to remold the known potent type I/II inhibitors into new type II inhibitors by replacing the BP fragments (Fig. 2). The combination gave several choices, and as listed in Table 1, we selected compound **5a** for further study.

3.2. Virtual simulation

Since the new compound is originally extracted and recombined from two types of ligands, docking simulation was primarily performed to predict the binding affinity difference between the ligands and the two types of proteins. In our assumption, the alteration of BP fragments shall lead to the increased binding affinity of ligand towards type II other than type I/II protein. Hence a preliminary docking simulation was carried out using both type II (PDB code: 3IDP) and type I/II (PDB code: 3C4C) B-Raf kinases as the receptors. Unsurprisingly, the binding affinities showed significant variation when the new compound docked into these two receptors (-Glide score for type II is 11.14 and for type I/II is 7.48). Thus, the result favored our design intention of recombining known inhibitors into new type II inhibitors.

As the preliminary simulation indicates the new compound may be a promising starting point, it was further substituted to afford a series of compounds. We also carried out docking simulation towards all the new compounds, as listed in Table 1. Overall, most compounds exhibited potent binding affinity to the receptor and especially compound **5h** (Fig. 3) has the most potent binding energy. Typically, compound **5h** hydrogen bonds with CYS532, THR529 and GLU501. Similar to the other type II compounds, residues VAL504, ILE572, HIS 574 and ASP594 also contribute to the binding affinity of **5h** with the target protein.

It is well acknowledged that docking simulation work should be employed with caution, for it generally focuses on a static binding mode prediction under vacuum condition. In light of this consideration, we utilized molecular dynamics simulation to evaluate the stabilization of the binding model. The results of root-mean-square deviation (RMSD) values were depicted in Fig. 4**A**. As shown, both the system and the ligand settled into equilibrium state soon, with smooth fluctuations under 0.3 nm and 0.1 nm, respectively. Also, the gyration radius values of the protein were recorded in Fig. 4**B**. Gyration radius (Rg) is an important measurement criterion to evaluate the compacting degree of protein and lower value reflects compacter state. The recorded total Rg slightly declined and remained stable during the simulation, hinting the protein kept a stable and compact state during the whole simulation. Together, the MD simulation provides a reliable verification of the binding model.

3.3. Chemical synthesis

The synthesis of target compounds followed the general pathway outlined in Fig. 5. All of the synthetic compounds are being

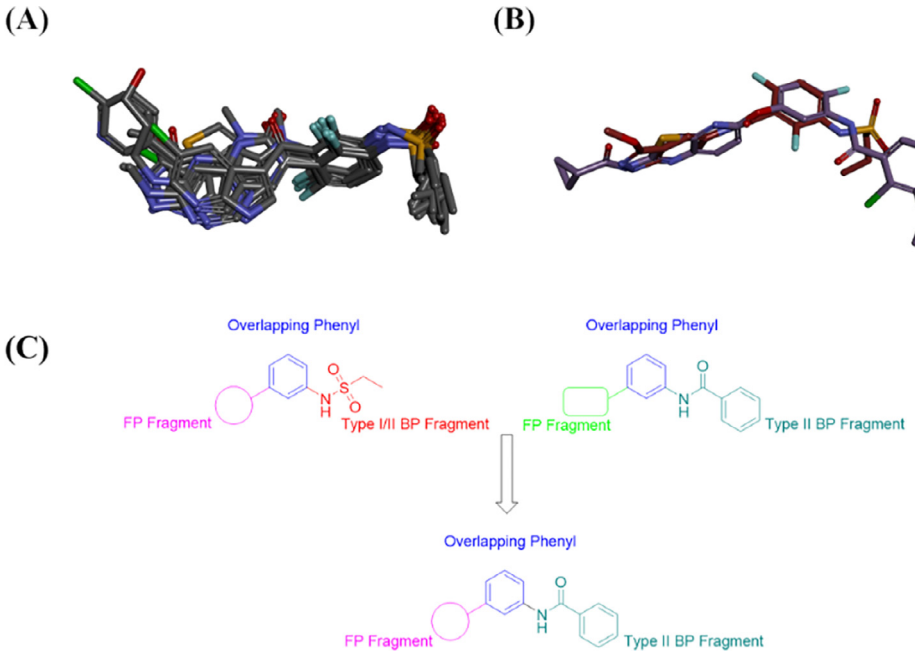

Fig. 2. Design of type II inhibitor based on type I/II inhibitor. (A) Type I/II inhibitors extracted from superimposed co-crystals. (B) Alignment of typical type I/II and type II inhibitors extracted from superimposed co-crystals. (C) Indication for the recombination of type I/II and type II inhibitors.

Table 1
The structures of compounds **5a-5t** and their binding scores on 3IDP and 3C4C

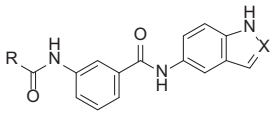

Compd	X	R	Glide scores		Compd	X	R	Glide scores	
			3IDP	3C4C				3IDP	3C4C
5a	N		11.14	7.48	**5k**	N		11.51	8.12
5b	N		10.49	8.59	**5L**	N		11.38	8.30
5c	N		10.55	9.17	**5m**	N		11.17	10.56
5d	N		11.41	9.51	**5n**	N		11.16	8.53
5e	N		11.23	9.77	**5o**	N	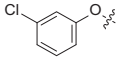	10.77	8.89
5f	N		11.62	8.84	**5p**	C		11.46	8.74
5g	N	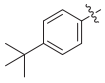	12.02	8.68	**5q**	C		11.10	8.67
5h	N	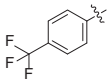	12.08	8.46	**5r**	C	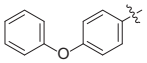	10.67	8.21
5i	N	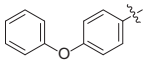	10.80	8.18	**5s**	C		11.25	8.97
5j	N		10.76	10.41	**5t**	C		10.20	7.77

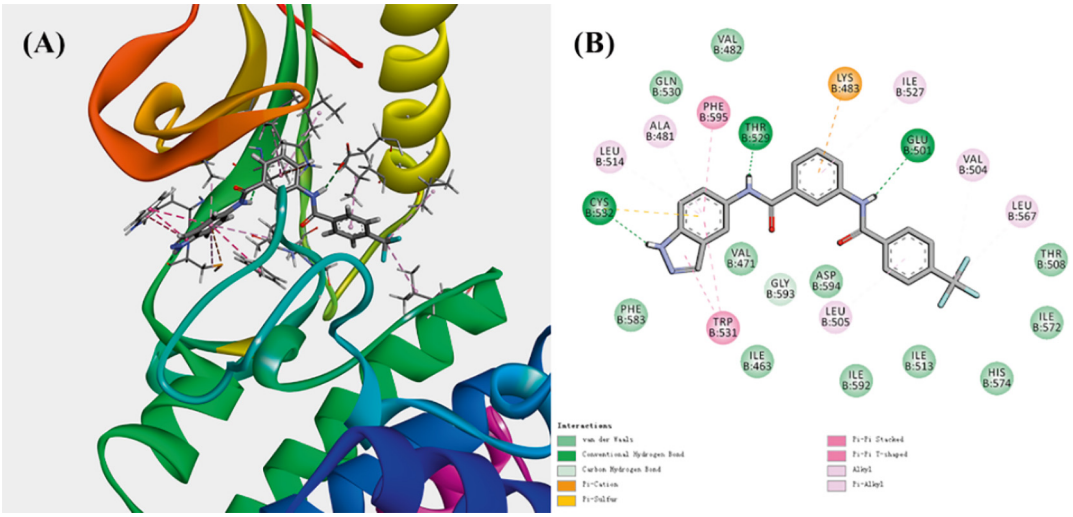

Fig. 3. The 3D (A) and 2D (B) binding modes of compound 5 h with type II B-Raf^{V600E} kinase 3IDP.

reported for the first time and gave satisfactory analytical and spectroscopic data. ^{1}HNMR, ESI-MS and element analysis spectra were in full accordance with the assigned structures.

3.4. Compound 5 h potently inhibited B-Raf^{V600E} kinase activity and proliferation of cancer cells

The inhibitory effects of all obtained compounds on kinase B-Raf^{WT} were evaluated, with sorafenib as a positive control drug. The results were summarized in Table 2. According to the results, most of the target compounds displayed good to excellent enzymatic inhibition to B-Raf^{V600E} kinase. Generally speaking, the kinase inhibitory effects of the tested compounds corresponded to their binding affinities with the type II protein 3IDP. While the *meta*- substitutions on the aryl R make no contribution to the activities (**5b** and **5c**), the *para*- substitutions usually give rise to an enhanced inhibition (**5d**-**5h**), compared to the starting compound **5a**. Especially, compound **5h** showed the best enzymatic

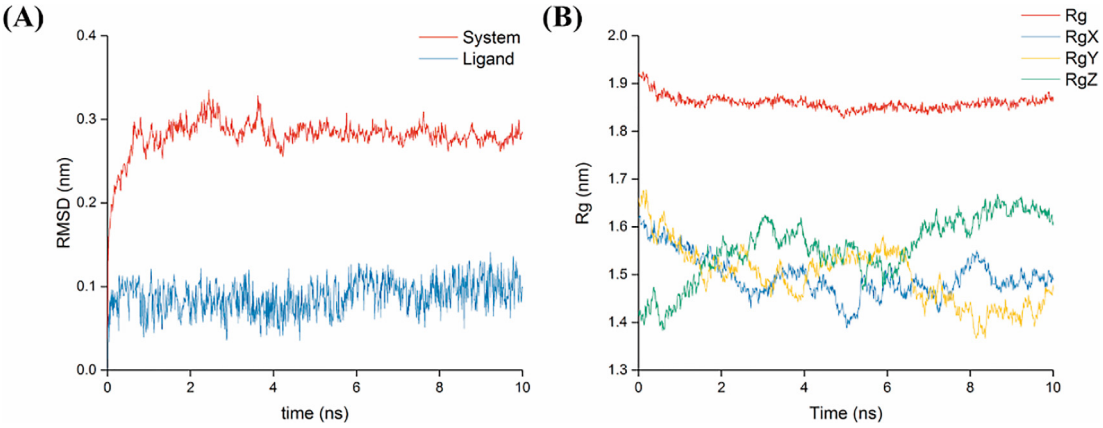

Fig. 4. Molecular dynamics simulation for compound 5 h binding with receptor. (A) The trajectory RMSD values for both system and ligand. (B) The gyration radius values for the receptor.

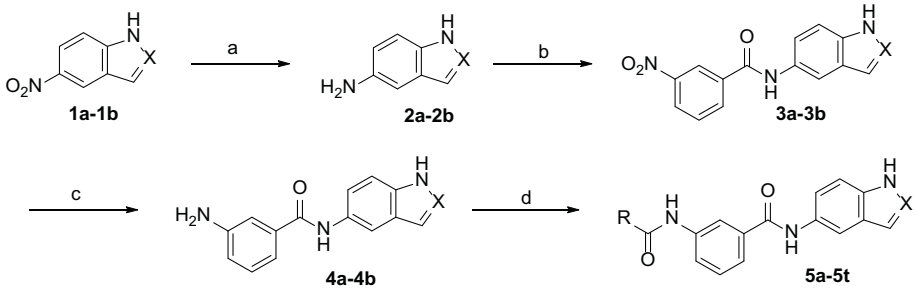

Fig. 5. The synthetic route for compounds 5a-5 t. (a) 80% Hydrazine hydrate, 10% Palladium charcoal, Ethanol, 80 °C, 10 min; (b) EDC, HOBT, DMAP, Et_3N, DMF, overnight; (c) 80% Hydrazine hydrate, 10% Palladium charcoal, Ethanol, 80 °C, 10 min; (d) EDC, HOBT, DMAP, Et_3N, DMF, overnight.

Table 2
In vitro antiproliferation activity of 5a-5 t towards cancer cells and inhibition activity towards B-Raf^{V600E} kinase.

Compounds	IC_{50} ± SD (μM)				
	HT29	HCT116	A375	WM-1361	B-Raf ^{V600E}
5a	16.11 ± 1.81	30.86 ± 2.15	9.12 ± 1.12	35.15 ± 2.70	5.22 ± 0.65
5b	19.15 ± 1.75	20.54 ± 1.47	12.21 ± 1.25	38.35 ± 2.86	8.71 ± 0.79
5c	20.54 ± 1.92	26.16 ± 2.72	9.87 ± 0.98	25.47 ± 1.75	4.94 ± 0.58
5d	12.23 ± 1.86	36.25 ± 3.51	7.15 ± 0.69	29.25 ± 1.94	1.57 ± 0.27
5e	17.85 ± 1.93	32.47 ± 3.05	7.62 ± 0.73	30.80 ± 2.58	3.04 ± 0.44
5f	14.40 ± 0.95	29.19 ± 2.50	5.74 ± 0.59	24.57 ± 2.05	2.78 ± 0.26
5g	10.86 ± 0.88	26.18 ± 2.33	2.85 ± 0.31	18.38 ± 1.41	0.75 ± 0.57
5h	4.41 ± 0.35	18.69 ± 1.91	1.97 ± 0.11	12.75 ± 1.22	0.18 ± 0.03
5i	18.52 ± 1.65	37.38 ± 3.01	9.45 ± 0.88	29.57 ± 2.06	5.27 ± 0.62
5j	17.19 ± 1.98	35.85 ± 2.78	8.29 ± 0.94	28.16 ± 1.98	4.11 ± 0.54
5k	11.51 ± 1.27	25.12 ± 2.02	7.46 ± 0.79	21.29 ± 2.33	0.81 ± 0.09
5L	12.24 ± 1.34	24.87 ± 1.25	8.83 ± 0.97	27.15 ± 2.17	1.05 ± 0.25
5m	9.65 ± 0.82	22.22 ± 2.49	7.58 ± 0.65	19.57 ± 1.72	0.46 ± 0.06
5n	8.99 ± 0.67	19.67 ± 1.78	4.56 ± 0.57	16.21 ± 1.11	1.14 ± 0.12
5o	16.70 ± 1.33	24.54 ± 2.41	10.18 ± 1.54	32.24 ± 3.27	5.32 ± 0.52
5p	10.62 ± 1.88	21.18 ± 1.70	6.49 ± 0.82	24.57 ± 2.54	2.11 ± 0.41
5q	11.11 ± 1.52	22.34 ± 2.35	6.72 ± 0.73	19.57 ± 1.75	2.61 ± 0.35
5r	21.09 ± 2.86	35.25 ± 2.74	10.45 ± 1.22	21.64 ± 2.07	5.72 ± 0.68
5s	10.58 ± 1.64	23.76 ± 2.53	5.78 ± 0.62	17.37 ± 1.62	3.52 ± 0.34
5t	19.56 ± 1.81	35.52 ± 2.57	8.46 ± 0.78	19.22 ± 1.84	6.57 ± 0.77
Sorafenib	8.44 ± 0.49	23.31 ± 1.38	3.36 ± 0.54	16.44 ± 1.35	0.13 ± 0.01

inhibition with IC_{50} values of 0.18 ± 0.03 μM. However, bulky substation group on the same position seems to attenuate the activity as **5i** only has a moderate activity. The same tendency is also true for the compounds with pyridine R group or carbon X group. In addition, it reveals that the pyridine R group shall be a better choice for compounds **5j**-**5n** showed better potential than their aryl analogs **5a-5f**. Hence, further modification may start with compounds bearing pyridine R group. As to the X group, most compounds with carbon atom (**5p-5t**) were less active than those with nitrogen atom (**5a**, **5e**, **5i**, **5j** and **5L**), suggesting a preference for the indazole instead of indole in structure.

Subsequently, the entities were evaluated by the MTT assay for anti-proliferation activity against four cancer cell lines, A375 (B-Raf^{V600E}), HT29 (B-Raf^{V600E}), WM1361 (B-Raf^{WT}), and HCT116 (B-Raf^{WT}). The IC_{50} values were calculated as listed in Table 2. To compound **5h**, it showed better suppression when exerting on

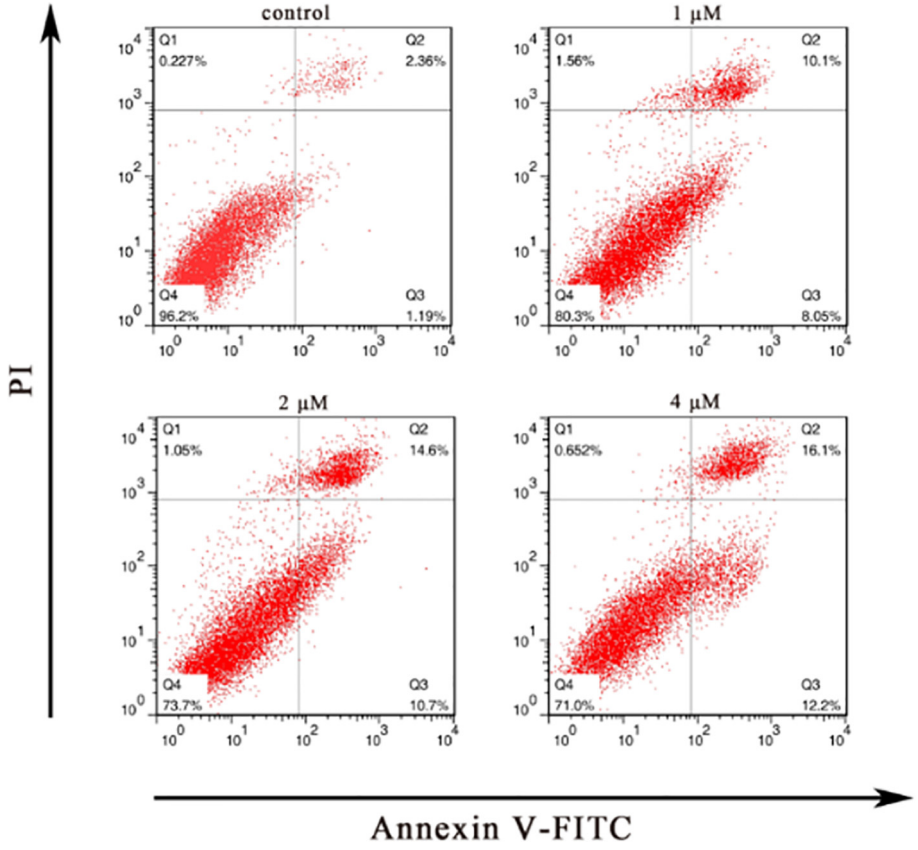

Fig. 6. Compound 5 h induced A375 cell apoptosis. A375 cells treated with 0, 1, 2 and 4 μM 5 h for 24 h were collected and analyzed. The percentage of early apoptotic cells was shown in the lower right quadrant (Annexin V-FITC positive/PI negative cells), and late apoptotic cells are located in the upper right quadrant (Annexin V-FITC positive/PI positive cells).

the A375 cells and HT29 cells for 48 h. To WM1361 and HCT116 cells expressing B-Raf^{WT}, the cell viability of cells treated with compound **5h** was significantly higher than that of cells carrying B-Raf^{V600E}. The MTT assays suggested that compound **5h** is a potential B-Raf^{V600E} inhibitor and could efficiently inhibit the proliferation of B-Raf^{V600E}-harbored cell lines.

3.5. Compound 5 h induced cell apoptosis in a dose-dependent manner

To determine whether compound **5h** induced cell apoptosis, an Annexin V/PI double staining assay was carried out. A375 cells were treated with increasing concentrations (0, 1, 2 and 4 μM) of **5h** for 24 h, followed by Annexin V/PI double staining and flow cytometric measurement. As shown in Fig. 6, the percentage of apoptotic cells dose-dependently elevated with the treatment of compound **5h**, and cell apoptotic rate reached up to 28.3% (sum of Q2 and Q3) when drug concentration increased to 4 μM. In short, compound **5h** could induce A375 cells apoptosis in a dose-dependent manner.

3.6. Compound 5 h could interfere the B-Raf^{V600E}-mediated pathways

While the abnormally activated ERK pathway caused by B-Raf^{V600E} results in the phosphorylated level of MEK and ERK increased, effective B-Raf^{V600E} inhibitors shall block the pathway and down-regulate the amount of pERK and pMEK. The effect of **5h** on ERK and MEK phosphorylation was investigated in A375 cell line expressing B-Raf^{V600E} and WM1361 cell line expressing B-Raf^{WT}. As shown in Fig. 7**(A), 5h** dose-dependently reduced the expression of the phosphorylation of ERK and MEK in A375 cells,

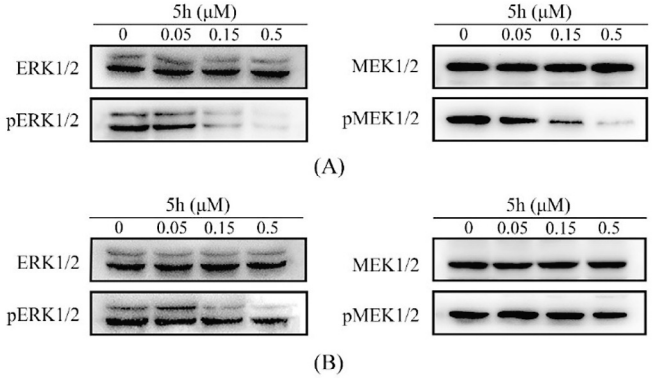

Fig. 7. Compound 5 h blocked the ERK and MEK pathway in A375 cells. (A) 5 h inhibited the phosphorylation of ERK and MEK in A375 melanoma cells bearing B-Raf^{V600E}; (B) 5 h slightly inhibited the phosphorylation of ERK and MEK in WM1361 melanoma cells bearing B-Raf^{WT}.

while the expression of total ERK or MEK protein levels was not affected. Subsequently, the inhibitory effect of **5h** to MEK and ERK phosphorylation in B-Raf^{WT} cell line WM1361 was assessed. The paradoxical effect of vemurafenib at different concentrations was reported as in the B-Raf^{WT} cells lower doses of vemurafenib give rise to the enhancing phosphorylation of ERK and MEK while higher doses block the phosphorylation of ERK and MEK. However, the treatment to WM1361 cells with lower doses of **5h** showed no significant inducing effect on the phosphorylation of ERK and MEK, as shown in Fig. 7**(B)**. Moreover, treatment with higher dose of **5h** slightly inhibited the phosphorylation of ERK and MEK. Together,

the results suggested that compound **5h** doesn't induce paradoxical effect in the normal cells.

4. Conclusion

In this study, we have combined molecular docking and molecular dynamics to fulfill the design and validation of hit compound, based on which we further synthesized a series of derivatives and evaluated their biological activities. Preliminary results showed that a few of the compounds displayed good inhibitory $BRAF^{V600E}$ activities and antiproliferation activities against A375 cell lines. Among these compounds, **5h** showed the most potent $BRAF^{V600E}$ inhibition activities with IC_{50} value of 0.18 ± 0.03 μM and antiproliferation activities with IC_{50} value of 1.97 ± 0.11 μM to A375 cells. Furthermore, mechanism of action studies proved that **5h** could induce apoptosis in A375 cells and interfere the $B\text{-}Raf^{V600E}$-mediated pathways. Our findings indicate that compound **5h** could be a lead molecule for further research into $BRAF^{V600E}$ inhibitors.

5. Disclosure of potential conflicts of interest

The authors disclose that there is no potential conflict of interest.

Acknowledgements

The work was financed by the Public Science and Technology Research Funds Projects of Ocean (No. 201505023), the International Postdoctoral Exchange Fellowship Program 2017 (No. 20170029) and Nanjing University Undergraduate Innovation Program and the National Natural Science Foundation of China (No. J1210026).

References

1. Fecher LA, Amaravadi RK, Flaherty KT. The MAPK pathway in melanoma. *Curr Opin Oncol*. 2008;20:183–189.
2. Wang P-F, Qiu H-Y, Wang Z-F, et al. Identification of novel B-Raf V600E inhibitors employing FBDD strategy. *Biochem Pharmacol*. 2017;132:63–76.
3. Davies H, Bignell GR, Cox C, et al. Mutations of the BRAF gene in human cancer. *Nature*. 2002;417:949–954.
4. Sharma A, Tran MA, Liang S, et al. Targeting mitogen-activated protein kinase/extracellular signal–regulated kinase kinase in the mutant (V600E) B-Raf signaling cascade effectively inhibits melanoma lung metastases. *Cancer Res*. 2006;66:8200–8209.
5. Yang Y-S, Zhang F, Tang D-J, Yang Y-H, Zhu H-L. Modification, Biological Evaluation and 3D QSAR Studies of Novel 2-(1, 3-Diaryl-4, 5-Dihydro-1H-Pyrazol-5-yl) Phenol Derivatives as Inhibitors of B-Raf Kinase. *PLoS ONE*. 2014;9:e95702.
6. Long GV, Stroyakovskiy D, Gogas H, et al. Combined BRAF and MEK inhibition versus BRAF inhibition alone in melanoma. *N Engl J Med*. 2014;371:1877–1888.
7. Corcoran RB, Dias-Santagata D, Bergethon K, Iafrate AJ, Settleman J, Engelman JA. BRAF gene amplification can promote acquired resistance to MEK inhibitors in cancer cells harboring the BRAF V600E mutation. *Sci Signal*. 2014;3(149):ra84.
8. Grbovic O, Basso A, Sawai A, et al. V600E B-Raf requires the Hsp90 chaperone for stability and is degraded in response to Hsp90 inhibitors. *PNAS*. 2006;103:57–62.
9. Li J, Feng J, Wang Y, et al. The B-RafV600E inhibitor dabrafenib selectively inhibits RIP3 and alleviates acetaminophen-induced liver injury. *Cell Death Dis*. 2014;5:e1278.
10. Murray CW, Rees DC. Opportunity Knocks: Organic Chemistry for Fragment-Based Drug Discovery (FBDD). *Angew Chem Int Ed*. 2016;55:488–492.
11. Jang S, Atkins M. Treatment of BRAF-mutant melanoma: the role of vemurafenib and other therapies. *Clin Pharmacol Ther*. 2014;95:24–31.
12. Wilhelm S, Carter C, Lynch M, et al. Discovery and development of sorafenib: a multikinase inhibitor for treating cancer. *Nat Rev Drug Discovery*. 2006;5:835–844.
13. Chapman PB, Hauschild A, Robert C, et al. Improved survival with vemurafenib in melanoma with BRAF V600E mutation. *N Engl J Med*. 2011;364:2507–2516.
14. Shi H, Moriceau G, Kong X, et al. Melanoma whole-exome sequencing identifies V600EB-RAF amplification-mediated acquired B-RAF inhibitor resistance. *Nat Commun*. 2012;3:724.
15. Thakur MD, Salangsang F, Landman AS, et al. Modelling vemurafenib resistance in melanoma reveals a strategy to forestall drug resistance. *Nature*. 2013;494:251–255.
16. Chapman P, Hauschild A, McArthur G. Vemurafenib in melanoma with BRAF V600E mutation. *N Engl J Med*. 2011;365:1448–1449.
17. Patrawala S, Puzanov I. Vemurafenib (RG67204, PLX4032): a potent, selective BRAF kinase inhibitor. *Future Oncol*. 2012;8:509–523.
18. Zhang C, Spevak W, Zhang Y, et al. RAF inhibitors that evade paradoxical MAPK pathway activation. *Nature*. 2015;526:583–586.
19. Arora R, Di Michele M, Stes E, et al. Structural investigation of B-Raf paradox breaker and inducer inhibitors. *J Med Chem*. 2015;58:1818–1831.
20. Verkhivker G. Molecular dynamics simulations and modelling of the residue interaction networks in the BRAF kinase complexes with small molecule inhibitors: probing the allosteric effects of ligand-induced kinase dimerization and paradoxical activation. *Mol BioSyst*. 2016;12:3146–3165.
21. Qiu H-Y, Fu J-Y, Yang M-K, et al. Identification of new shikonin derivatives as STAT3 inhibitors. *Biochem Pharmacol*. 2017;146:74–86.
22. Qiu H-Y, Zhu X, Luo Y-L, et al. Identification of New Shikonin derivatives as antitumor agents targeting STAT3 SH2 domain. *Sci Rep*. 2017;7:2863.
23. Van Linden OP, Kooistra AJ, Leurs R, de Esch IJ, de Graaf C. KLIFS: a knowledge-based structural database to navigate kinase–ligand interaction space. *J Med Chem*. 2013;57:249–277.
24. Kooistra AJ, Kanev GK, van Linden OP, Leurs R, de Esch IJ, de Graaf C. KLIFS: a structural kinase-ligand interaction database. *Nucleic Acids Res*. 2015;44:D365–D371.